Stabilization of the Quantum Spin Hall Effect by Designed Removal of Time-Reversal Symmetry of Edge States

Huichao Li, L. Sheng, R. Shen, L. B. Shao, Baigeng Wang, D. N. Sheng, and D. Y. Xing

Phys. Rev. Lett. **110**, 266802 — Published 24 June 2013

DOI: 10.1103/PhysRevLett.110.266802

Stabilization of Quantum Spin Hall Effect by Designed Removal of Time-Reversal Symmetry of Edge States

Huichao Li[1], L. Sheng[1],* R. Shen[1], L. B. Shao[1], Baigeng Wang[1], D. N. Sheng[2], and D. Y. Xing[1]†
[1]*National Laboratory of Solid State Microstructures and Department of Physics, Nanjing University, Nanjing 210093, China*
[2] *Department of Physics and Astronomy, California State University, Northridge, California 91330, USA*

The quantum spin Hall (QSH) effect is known to be unstable to perturbations violating time-reversal symmetry. We show that creating a narrow ferromagnetic (FM) region near the edge of a QSH sample can push one of the counterpropagating edge states to the inner boundary of the FM region, and leave the other at the outer boundary, without changing their spin polarizations and propagation directions. Since the two edge states are spatially separated into different "lanes", the QSH effect becomes robust against symmetry-breaking perturbations.

PACS numbers: 72.25.-b, 73.43.-f, 73.20.At, 73.50.-h

The quantum spin Hall (QSH) effect, a quantum state of matter, has attracted much attention in recent years, because of its fundamental interest and potential applications in spintronic devices. The QSH effect was first predicted theoretically by Kane and Mele [1] and by Bernevig and Zhang [2], in independent works. Soon after, the QSH effect was observed experimentally in HgTe quantum wells, [3] following theoretical prediction. [4] The discovery of the QSH effect has inspired the theoretical proposals [5–9] for topological insulators in three dimension, which have been confirmed experimentally. [10–15] A key ingredient to the QSH effect is a strong intrinsic spin-orbit coupling, which acts as spin-dependent magnetic fluxes coupled to the electron momentum. In the ideal case, where electron spin is conserved, the two spin sectors of a QSH system behave like two independent quantum Hall (QH) systems without Landau levels. [16] They contribute opposite quantized Hall conductivities, when the electron Fermi level is inside the bulk band gap, so that the total Hall conductivity vanishes but the spin Hall conductivity is quantized. On a sample edge, two counterpropagating gapless edge modes with opposite spin polarizations exist in the bulk band gap, which can transport spin currents without dissipation of energy.

When the spin conservation is destroyed, e.g., by the Rashba-like spin-orbit coupling, the spin Hall conductivity deviates from the quantized value. [17] However, the edge transport can remain to be dissipationless, [1, 18] provided that the time-reversal (TR) symmetry is present and the bulk band gap is not closed. In this case, a QSH system can no longer be divided into two QH systems, and the existence of the gapless edge states has been attributed to the nontrivial topological properties of bulk energy bands. The nontrivial bulk band topology of the QSH systems is usually described by the Z_2 index [19] or the spin Chern numbers. [20–22]

While the TR symmetry was often considered to be a prerequisite to the QSH effect, its role is two-sided. In a TR invariant QSH system, the two oppositely moving edge states at the Fermi energy are connected to each other under TR, and so have opposite spin orientations. Elastic backscattering from nonmagnetic random potential is forbidden. On the other hand, the two opposite movers have identical spatial probability distributions. Turning on small TR-symmetry-breaking perturbations immediately couples the two edge states, giving rise to backscattering. This makes the QSH effect fragile in realistic environments, where perturbations violating the TR symmetry are usually unavoidable. Experimentally, two-terminal conductance close to the predicted value $2(e^2/h)$ was observed only for small QSH samples with dimensions of about $(1 \times 1)\mu m^2$, [3] in contrast to the traditional QH effect, where the Hall conductivity can be precisely quantized on macroscopic scales. So far, QSH effect as robust as the QH effect has been elusive. It was found recently that the nontrivial bulk band topology of the QSH systems remains intact, even when the TR symmetry is broken, [23] implying that the instability of the QSH effect is solely due to properties of the edge states.

In this Letter, we show that the QSH effect can be stabilized in two-dimensional topological insulators by inducing ferromagnetism on narrow strips along the edges. As a result of the quantum anomalous Hall (QAH) effect generated by the exchange field [24] within a ferromagnetic (FM) strip, one of the helical edge states is pushed to the inner boundary of the FM region, and the other remains on the outer boundary. The moving directions and spin orientations of the individual edge states are unchanged, so that the QSH effect persists. Importantly, the edge states are spatially separated, so that the QSH effect becomes robust against general perturbations without fictitious symmetry constraints. We present both qualitative discussion and quantitative calculation to demonstrate the physical picture and practical feasibility of this proposal. Our work paves a road to realize robust QSH effect via magnetic manipulation.

We start from the effective Hamiltonian for a HgTe quantum well [4] with an exchange field given by $H = H_0 + H_1$ with

$$H_0 = v_{\rm F}(\hat{\tau}_z k_x \hat{\sigma}_x + k_y \hat{\sigma}_y) + Dk^2 + (M_0 - Bk^2)\hat{\sigma}_z \ . \quad (1)$$

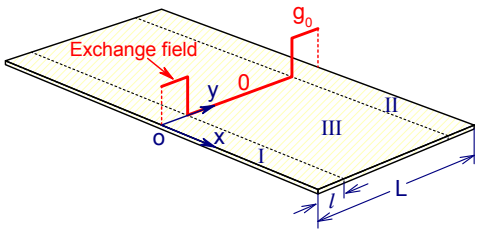

FIG. 1: Schematic of the QSH sample with a long strip geometry. The profile of the y-dependent exchange field is shown by the thick (red) line.

Here, $v_{\rm F}$, D, M_0 and B are the parameters of the model, $\hat{\boldsymbol{\tau}}$ stand for Pauli matrices for two spin states, and $\hat{\boldsymbol{\sigma}}$ for the electron and hole bands. An exchange field can be created in the HgTe layer by doping of magnetic atoms, such as Mn. [24] Within the mean-field approximation, the exchange field can be described by [24] $H_1 = (g_0\hat{\sigma}_z + g_1)\hat{\tau}_z$, where $g_0 = \frac{1}{2}(G_{\rm H} - G_{\rm E})$ and $g_1 = \frac{1}{2}(G_{\rm H} + G_{\rm E})$ with $2G_{\rm E}$ ($2G_{\rm H}$) as the exchange splitting of the electron (hole) bands. For convenience, we set the reduced Planck constant $\hbar$ to be unity. $B^2 > D^2$ is assumed to ensure the valence bands to be inverted. [22, 25]

Since $\hat{\tau}_z$ is a conserved quantity, one can easily diagonalize Eq. (1), and obtain two conduction bands and two valence bands. Under the condition of $|g_1| < \max(|M_0|, |g_0|)$, a nonzero middle band gap exists, except at $g_0 = \pm M_0$ where the conduction and valence bands touch; otherwise the conduction and valence bands overlap and the system is a metal. As has been discussed in Ref. [24], for HgTe quantum wells doped with Mn, $G_{\rm E}$ and $G_{\rm H}$ have opposite signs, so that the above condition is satisfied. Given $|g_1| < \max(|M_0|, |g_0|)$, the spin Chern numbers for $\tau_z = \pm 1$ can be derived to be $C_\pm = \pm\frac{1}{2}[\mathrm{sgn}(B) + \mathrm{sgn}(M_0 \pm g_0)]$. At $g_0 = 0$, $C_\pm = \pm\mathrm{sgn}(B)$ if $BM_0 > 0$, corresponding to a QSH phase, and $C_\pm = 0$ if $BM_0 < 0$, corresponding to an ordinary insulator. We focus on systems with $BM_0 > 0$, and for the sake of definiteness, we will confine ourselves to the parameter region of $B < 0$ and $M_0 < 0$, which is the case with the HgTe quantum wells exhibiting the QSH effect. (All the conclusions reached in this work do also apply to $B > 0$ and $M_0 > 0$.) In this case, $C_\pm = (-1, 1)$ at $g_0 = 0$. With increasing g_0 to $g_0 = |M_0|$, $C_\pm$ undergo a transition from $(-1, 1)$ to $(0, 1)$, the latter corresponding to a QAH phase. [23, 24]

Next we consider a QSH sample with a strip geometry, as shown in Fig. 1. Since $C_\pm$ do not depend on D and g_1 for $|g_1| < \max(|M_0|, |g_0|)$, without loss of generality, we set $D = g_1 = 0$ for now to make a physical discussion, and the effect of finite D and g_1 will be taken into account in numerical calculation later. The exchange field g_0 is taken to be nonzero in region I of $0 < y < l$ and region II of $(L - l) < y < L$, and vanishing in region III of $l < y < (L - l)$. The system as a whole has a bulk

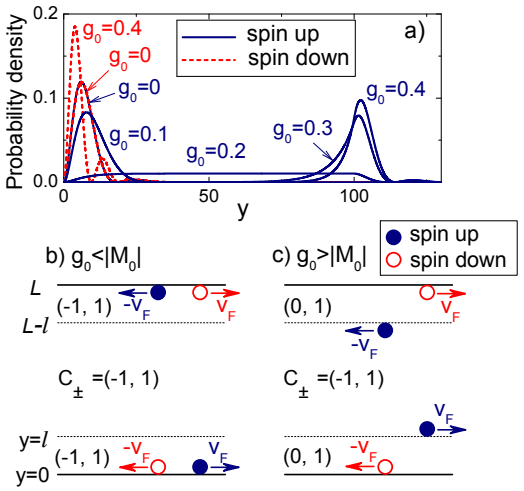

FIG. 2: (a) $|\phi_+(k_x, y)|^2$ and $|\phi_-(k_x, y)|^2$ at $k_x = 0$ as functions of y for different g_0, where $v_{\rm F} = 1$, $B = -5$, $M_0 = -0.2$, and $l = 100$ are taken. (b,c) Spatial distributions of spin Chern numbers $C_\pm$ and edge states for $g_0 < |M_0|$ and $g_0 > |M_0|$.

energy gap around energy 0, for $g_0 \neq \pm M_0$. The edge states in the bulk energy gap can be solved analytically by replacing k_y with $-i\partial_y$ in the system Hamiltonian. For $\tau_z = 1$, an edge mode with energy $E_+(k_x) = v_{\rm F}k_x$ is found on one side of the strip, whose wavefunction is given by

$$\varphi_+(k_x, y) = |1, 1\rangle\phi_+(k_x, y) \ . \tag{2}$$

Here, ket $|\tau_z, \sigma_x\rangle$ with $\tau_z = \pm 1$ and $\sigma_x = \pm 1$ is used to represent the common eigenstate of $\hat{\tau}_z$ and $\hat{\sigma}_x$. The spatial wavefunction $\phi_+(k_x, y) = C[e^{-y/\xi_1(g_0)} - e^{-y/\xi_2(g_0)}]$ for $y < l$, and $\phi_+(k_x, y) = D_1 e^{-(y-l)/\xi_1(0)} - D_2 e^{-(y-l)/\xi_2(0)}$ for $y \geq l$, with C, D_1 and D_2 to be determined from the conditions of continuity and normalization of $\phi_+(k_x, y)$. The two characteristic length functions are defined as

$$\xi_{1,2}(\epsilon) = \frac{2|B|}{v_{\rm F} \pm \sqrt{v_{\rm F}^2 - 4B(M_0 - Bk_x^2 + \epsilon)}} \ . \tag{3}$$

For $\tau_z = -1$, we find another edge mode with energy $E_-(k_x) = -v_{\rm F}k_x$ and wavefunction

$$\varphi_-(k_x, y) = |-1, 1\rangle\phi_-(k_x, y) \ , \tag{4}$$

where $\phi_-(k_x, y) = E[e^{-y/\xi_1(-g_0)} - e^{-y/\xi_2(-g_0)}]$ for $y < l$, and $\phi_-(k_x, y) = F_1 e^{-(y-l)/\xi_1(0)} - F_2 e^{-(y-l)/\xi_2(0)}$ for $y \geq l$. Owing to the two-fold rotation symmetry, the edge modes on the other side of the strip have dispersion relations $E_\pm(k_x) = \mp v_{\rm F}k_x$.

In Eqs. (2) and (4), the $\hat{\boldsymbol{\tau}}$ and $\hat{\boldsymbol{\sigma}}$ parts of wavefunctions do not change with varying g_0. In Fig. 2(a), the modulus squared of spatial wavefunctions $\phi_+(0, y)$ and $\phi_-(0, y)$ are plotted as functions of y for several values

of g_0. Here, the momentum is taken to be dimensionless by properly choosing the units for $v_{\rm F}$ and B, and $v_{\rm F}$ is used as the unit of energy. At $g_0 = 0$, we have $|\phi_+(0,y)|^2 = |\phi_-(0,y)|^2$, and both lines coincide with each other, which is required by the TR symmetry at $g_0 = 0$, as mentioned above. With increasing g_0, the peak of $|\phi_-(0,y)|^2$ becomes sharper and closer to $y = 0$. On the contrary, the shape of $|\phi_+(0,y)|^2$ widens with increasing g_0, and spreads across region I at $g_0 = |M_0| = 0.2$. With further increasing g_0, $|\phi_+(0,y)|^2$ becomes localized near $y = l = 100$, i.e., the inner boundary of region I.

The evolution of the edge states with varying g_0 is further illustrated in Figs. 2(b) and 2(c), and can be understood in terms of calculated spin Chern numbers. For $g_0 < |M_0|$, the spin Chern numbers $C_\pm$ in the three regions take the same value $(-1, 1)$. This indicates that the three regions are topologically equivalent, and can be regarded as a QSH system as a whole. As a result, the edge states for both up spin ($\tau_z = 1$) and down spin ($\tau_z = -1$) appear near the sample boundaries $y = 0$ and $y = L$, as shown in Fig. 2(b). For $g_0 > |M_0|$, the situation is quite different, because $C_\pm$ undergo a transition at $g_0 = |M_0|$ from $(-1, 1)$ to $(0, 1)$ in regions I and II, corresponding to a QAH phase. [23, 24] For the spin-down electrons, the three regions have the same Chern number $C_- = 1$, and as a whole are equivalent to a QH system. Therefore, the spin-down edge states remain localized near $y = 0$ and $y = L$. For the spin-up electrons, region III with $C_+ = -1$ is a QH system, sandwiched between two insulators in regions I and II, where $C_+ = 0$. The spin-up edge states thus shift to their interfaces, namely, $y = l$ and $y = L - l$, as shown in Fig. 2(c). Comparing Fig. 2(c) for $g_0 > |M_0|$ with Fig. 2(b) for $g_0 < |M_0|$, one finds that both systems have very similar edge states, so as to exhibit the same QSH effect. An important difference is that for $g_0 > |M_0|$, the counterflows of electrons at the lower (upper) edge are spatially separated into two different "lanes" located at $y = 0$ ($y = L$) and $y = l$ ($y = L-l$), which provides an essential protection for the edge states against backscattering from symmetry-breaking random potential.

We have shown how the QSH effect can be strengthened by doping of magnetic atoms near the edges of a QSH system. Now we consider a more realistic model for HgTe quantum wells doped with Mn atoms ($Hg_{1-c}Mn_cTe$), for which Hamiltonian H_0 is still given by Eq. (1). However, we take into account the fact that the doped Mn atoms are spatially randomly distributed, and their spins may not be fully aligned, so that H_1 is taken to be

$$H_1 = -\frac{1}{\pi\lambda^2}\sum_{\alpha=0}^{N_{\rm Mn}-1}(j_0\hat{\sigma}_z + j_1)\hat{\boldsymbol{\tau}}\cdot\mathbf{s}_\alpha \exp\left(-|\mathbf{r}-\mathbf{R}_\alpha|^2/\lambda^2\right) . \quad (5)$$

Here, factor $(j_0\hat{\sigma}_z + j_1)$ accounts for different electron-spin interaction strengths in the electron and hole bands, $\mathbf{r}$ is the electron coordinate operator, $\mathbf{R}_\alpha$ the position of the α-th Mn atom, and $N_{\rm Mn}$ the total number of the Mn atoms. The local spins ($S = 5/2$) of the Mn atoms are treated as classical vectors, and $\mathbf{s}_\alpha$ is a unit vector in the direction of the local spin of the α-th Mn atom. The distribution of the orientations of the local spins is assumed to be Boltzmann-Maxwell-like [26] $f(\mathbf{s}_\alpha) \propto e^{-\eta\cos\theta_\alpha}$, where θ_α is the polar angle of $\mathbf{s}_\alpha$, and η is a parameter which can be related to the ratio of magnetization M to saturated magnetization M_s: $M/M_s = -\langle\cos\theta_\alpha\rangle = \coth(\eta) - 1/\eta$. Therefore, for a given ratio M/M_s, the distribution is fully determined. We will set $M = M_s/3$, for which the local spins are randomly oriented to a large degree. As a result, H_1 given by Eq. (5) not only provides an exchange field, but also acts as a scattering potential of magnetic impurities. If one makes the mean-field approximation, by replacing $\mathbf{s}_\alpha$ with its average $\langle\mathbf{s}_\alpha\rangle = -(M/M_s)\mathbf{e}_z$ and averaging Eq. (5) over a random distribution of $\mathbf{R}_\alpha$, Eq. (5) recovers $H_1 = (g_0\hat{\sigma}_z + g_1)\hat{\tau}_z$, where $g_0 = j_0 cM/M_s a_0^2$ and $g_1 = j_1 cM/M_s a_0^2$ with a_0 as the lattice constant. By using the known expressions for mean-field parameters g_0 and g_1, [24] we get $j_0 = 464\text{meV}\cdot\text{nm}^2$ and $j_1 = 286\text{meV}\cdot\text{nm}^2$, which are independent of M/M_s and doping concentration c, as g_0 and g_1 are proportional to cM/M_s. The coupling range λ is set to be 10nm. [27]

The other parameters of the model are taken from Ref. [28] $v_{\rm F} = 364.5\text{meV}\cdot\text{nm}$, $B = -686\text{meV}\cdot\text{nm}^2$, $D = -512\text{meV}\cdot\text{nm}^2$, and $M_0 = -10$meV, corresponding to a HgTe quantum well of thickness 7.0nm. We consider a sample having the strip geometry shown in Fig. (1), with linear sizes $L_x = 80$nm and $L = 560$nm in the x and y directions. The doped Mn atoms are randomly distributed in regions of width $l = 80$nm near the two edges, with potential described by Eq. (5). We employ the supercell algorithm, [29] in which the $L_x \times L$ sample (supercell) is duplicated along the x direction to form a superlattice. A tight-binding model on square meshes is constructed, which recovers the form of Eq. (1) in the continuum limit. The eigenenergies of the superlattice as functions of the longitudinal momentum [30] q_x are calculated by exact diagonalization, and the result for four different doping concentrations is plotted in Figs. 3(a-d). The mesh size is set to be 4nm, and good convergence is verified with smaller mesh sizes. For $c = 0.005$, apparent energy gaps exist in the edge state spectrum, indicating the occurrence of backscattering. With increasing c to 0.01, the energy gaps decrease but remain finite. With further increasing c to 0.02 and 0.03, the energy gaps essentially vanish, an indication of quenching of backscattering.

At a given Fermi energy $E_F = 4$meV, the typical spatial probability distributions of the edge states on an arbitrarily chosen cross-section of the sample for different doping concentrations are plotted in Figs. 3(e-h), in which only the profile on one side of the sample is shown. For $c = 0.005$, the spin-up and spin-down polarized edge

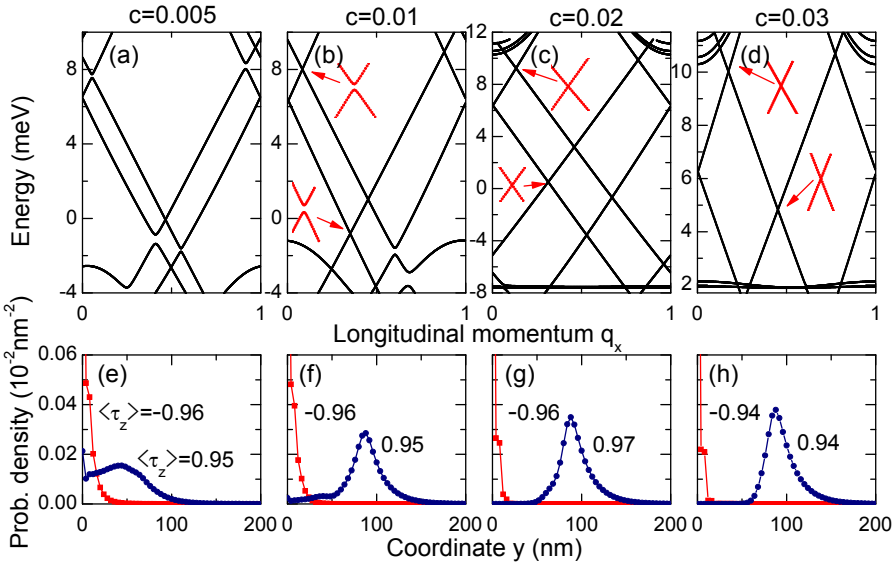

FIG. 3: (a-d) Calculated eigenenergies for four different doping concentrations as functions of momentum q_x (in units of $2\pi/L_x$). (e-h) Corresponding probability density distributions of the edge states at $E_F = 4$meV, which is normalized in the $L_x \times L$ sample. The spin polarizations $\langle\hat{\tau}_z\rangle$ of the edge states are indicated in (e-h).

states both located at $y = 0$ have a large spatial overlap. For $c = 0.01$, while the spin-down edge state remains to be near $y = 0$, the spin-up edge state moves away from $y = 0$ toward $y = l = 80$nm. However, an appreciable overlap still exists between the two edge states, which is the origin of finite energy gaps for the edge state spectra in Figs. 3(a) and 3(b). With increasing c to 0.02 and 0.03, the spin-up edge state is peaked at $y = l$, and there is no longer overlap between the spin-up and spin-down edge states, as shown in Figs. 3(g) and 3(h). This accounts for the vanishing energy gaps of the edge states shown in Figs. 3(c) and 3(d). In conclusion, we have shown that robust QSH effect can be realized by placing random Mn impurities on the edge strips. In principle this leads to conflicting effects: on one hand the induced exchange field pulls apart the opposite spin edge channels, but on the other hand it provides a mechanism for backscattering by magnetic impurities. The present calculation, for realistic parameters of HgTe quantum wells, implies that the combined effect is stabilizing the QSH effect rather than vice versa.

This work is supported by the State Key Program for Basic Researches of China under Grants Nos. 2009CB929504 (LS), 2011CB922103, and 2010CB923400 (DYX), the National Natural Science Foundation of China under Grant Nos. 11225420, 11074110 (LS), 11174125, 11074109, 91021003 (DYX), and a project funded by the PAPD of Jiangsu Higher Education Institutions. We also thank the US NSF Grants No. DMR-0906816 and No. DMR-1205734, and Princeton MRSEC Grant No. DMR-0819860 (DNS).

* Electronic address: shengli@nju.edu.cn
† Electronic address: dyxing@nju.edu.cn

[1] C. L. Kane and E. J. Mele, Phys. Rev. Lett. **95**, 226801 (2005).
[2] B. A. Bernevig, and S. C. Zhang, Phys. Rev. Lett. **96**, 106802 (2006).
[3] M. König, *et al.*, Science **318**, 5851, 766 (2007).
[4] B. A. Bernevig, T. L. Hughes, and S. C. Zhang, Science **314**, 1757 (2006).
[5] J. E. Moore, and L. Balents, Phys. Rev. B **75**, 121306 (R) (2007).
[6] L. Fu and C. L. Kane, Phys. Rev. B **76**, 045302 (2007); L. Fu, C. L. Kane, E. J. Mele, Phys. Rev. Lett. **98**, 106803 (2007).
[7] H. J. Zhang, C. X. Liu, X. L. Qi, X. Dai, Z, Fang, and S. C. Zhang, Nature Phys. **5**, 438(2009).
[8] M. Z. Hasan and C. L. Kane, Rev. Mod. Phys. **82**, 3045 (2010).
[9] X. L. Qi and S. C. Zhang, Physics Today. **63**, 33 (2010).
[10] D. Hsieh, *et al.*, Nature **452**, 970 (2008); D. Hsieh, *et al.*, Science **323**, 919 (2009).
[11] Y. Xia, et al., Nature Physics 5, 398 (2009).
[12] H. Zhang, C. Liu, X. Qi, X. Dai, Z. Fang, and S. Zhang, Nature Physics **5**, 438 (2009).
[13] Y. L. Chen, *et al.*, Science **325**, 178 (2009).
[14] P. Roushan, *et al.*, Nature **460**, 1106 (2009).
[15] T. Zhang, *et al.*, Phys. Rev. Lett. **103**, 266803 (2009). Lett. 102, 146805 (2009).
[16] F. D. M. Haldane, Phys. Rev. Lett. **61**, 2015 (1988).
[17] L. Sheng, D. N. Sheng, C. S. Ting, and F. D. M. Haldane Phys. Rev. Lett. **95**, 136602 (2005).
[18] C. Wu, B. A. Bernevig, and S. C. Zhang Phys. Rev. Lett. **96**, 106401 (2006).
[19] C. L. Kane, and E. J. Mele, Phys. Rev. Lett. **95**, 146802 (2005).

[20] D. N. Sheng, Z. Y. Weng, L. Sheng, and F. D. M. Haldane, Phys. Rev. Lett. **97**, 036808 (2006).
[21] E. Prodan, Phys. Rev. B **80**, 125327 (2009); E. Prodan, New J. Phys. **12**, 065003 (2010).
[22] H. C. Li, L. Sheng, D. N. Sheng, and D. Y. Xing, Phys. Rev. B **82**, 165104 (2010).
[23] Y. Yang, Z. Xu, L. Sheng, B. G. Wang, D. Y. Xing, and D. N. Sheng Phys. Rev. Lett. **107**, 066602 (2011); H. C. Li, L. Sheng, and D.Y. Xing, Phys. Rev. Lett. **108**, 196806 (2012).
[24] C.-X. Liu, X.-L. Qi, X. Dai, Z. Fang, and S. C. Zhang, Phys. Rev. Lett. 101, 146802 (2008).
[25] W.-Y. Shan, H.-Z. Lu, S.-Q. Shen, New J. Phys. **12**, 043048 (2010); H.-Z. Lu, W.-Y. Shan, W. Yao, Q. Niu, and S.-Q. Shen, Phys. Rev. B **81**, 115407 (2010).
[26] L. Sheng, D. Y. Xing, D. N. Sheng, and C. S. Ting, Phys. Rev. Lett. **79**, 1710 (1997).
[27] Q. Liu *et al.*, Phys. Rev. Lett. **102**, 156603 (2009).
[28] M. König *et al.*, J. Phys. Soc. Japan **77**, 031007 (2008).
[29] D. L. Smith, and C. Mailhiot, Rev. Mod. Phys. **62**, 173 (1990).
[30] The longitudinal momentum in the supercell model is equivalent to the magnetic flux in the Laughlin gedanken experiment [R. B. Laughlin, Phys. Rev. B **23**, 5632 (1981)]. Given this equivalence, both systems have an identical energy spectrum.